Flame Retardancy and Water Resistance of Novel Intumescent Flame-Retardant Oil-Filled Styrene–Ethylene–Butadiene–Styrene Block Copolymer/Polypropylene Composites

Yuansheng Zang, Bin Li, Miaojun Xu

Heilongjiang Key Laboratory of Molecular Design and Preparation of Flame Retarded Materials, College of Science, Northeast Forestry University, Harbin 150040, People's Republic of China
Correspondence to: B. Li (E-mail: libinzh62@163.com)

ABSTRACT: A novel halogen-free flame-retardant composite consisting of an intumescent flame retardant (IFR), oil-filled styrene–ethylene–butadiene–styrene block copolymer (O-SEBS), and polypropylene (PP) was studied. On the basis of UL-94 ratings and limiting oxygen index (LOI) data, the IFRs consisted of a charring–foaming agent, ammonium polyphosphate, and SiO_2 showed very effective flame retardancy and good water resistance in the IFR O-SEBS/PP composite. When the loading of IFR was only 28 wt %, the IFR–O-SEBS/PP composite could still attain a UL-94 V-0 (1.6 mm) rating, and its LOI value remained at 29.8% after a water treatment at 70°C for 168 h. Thermogravimetric analysis data indicated that the IFR effectively enhanced the temperature of the main thermal degradation peak of the IFR–O-SEBS/PP composites because of the formation of abundant char residue. The flammability parameters of the composites obtained from cone calorimetry testing demonstrated that water treatment almost did not affect the flammability behavior of the composite. The morphological structures of the char residue and fractured surfaces of the composites were not affected by the water treatment. This was attributed to a small quantity of IFR extracted from the composite. © 2013 Wiley Periodicals, Inc. J. Appl. Polym. Sci. **2014**, *131*, 39575.

INTRODUCTION

Styrene–ethylene–butadiene–styrene block copolymer (SEBS) is a new thermoplastic elastomer. It is used extensively in many industrial applications, including wires and cables, household goods, sealing materials, medical materials, and electrical devices,[1,2] because of its high performance, including excellent mechanical properties and electrical properties, ozone resistance, UV resistance, oil resistance, and excellent low-temperature resistance.[3–7] Polypropylene (PP) is one of the most widely used polyolefin polymers because of its versatility and a good performance-to-cost ratio. In recent years, blends of SEBS and PP, especially oil-filled styrene–ethylene–butadiene–styrene block copolymer (O-SEBS)/PP composites, have been used widely in the wire and cable and automobile industries because of their excellent mechanical properties, processing properties, and aging resistance.[8–12]

However, O-SEBS-based composites can easily catch fire; this has resulted in serious restriction to their many applications.[13] So far, there have been some reports[13–16] on the halogen-free flame retardancy of SEBS-based composites.

Metal hydroxides,[13,14] red phosphorous,[15] expandable graphite,[14] and intumescent flame retardants (IFRs)[16] have been used as halogen-free flame retardants of O-SEBS/PP composites. Metal hydroxides, such as aluminum hydroxide and magnesium hydroxide, are both nontoxic and smoke-suppressing additives, but because of their low flame-retardant efficiency and high addition, the mechanical properties and processing ability of their composites are acutely destroyed. Red phosphorus is an efficient flame retardant; however, because of its dark color and the release of poisonous phosphine during processing, so applications are also obviously limited. Expandable graphite is an environmentally friendly flame retardant, but its application is also limited because of its dark color and high addition.

IFR technology first appeared in the 1980s.[17,18] In recent years, IFRs have been well known as high-efficiency flame retardants for elastomers and thermoplastics[19–24] because of some of their virtues, such as the very low amounts of smoke and nontoxic gases produced during burning and their antidripping properties. Generally, IFRs consist of three parts: an acid source, a

Table I. Components of the IFR–O-SEBS/PP Composites

Samples	Components of the composites			IFR components			
	O-SEBS (wt %)	PP (wt %)	IFR (wt %)	APP (wt %)	CFA (wt %)	SiO$_2$ (wt %)	Antidripping agent (wt %)
A	33.30	66.70	0	0	0	0	0
B	24.00	48.00	28	17.70	8.85	1.40	0.05
C	24.00	48.00	28	19.91	6.64	1.40	0.05
D	24.00	48.00	28	21.24	5.31	1.40	0.05
E	24.00	48.00	28	22.12	4.43	1.40	0.05
F	26.67	53.33	20	15.16	3.79	1.00	0.05
G	26.00	52.00	22	16.68	4.17	1.10	0.05
H	25.00	50.00	25	18.96	4.74	1.25	0.05
I	23.33	46.67	30	22.76	5.69	1.50	0.05

char-forming agent, and a blowing agent.[25–28] In recent years, many novel IFR systems have been studied, for example, triazine-ring-based macromolecular charring agents[29,30] and the pentaerythritol phosphate based char source.[31,32] The former presents better comprehensive properties, including flame retardancy, water resistance, and thermal stability for PP; these were reported in our previous work.[29,30,33,34] However, triazine macromolecules containing IFR have not been systematically investigated in the O-SEBS/PP system. We hope that IFRs can be adopted in the flame-retardant O-SEBS/PP system.

In this study, the IFR consisted of ammonium polyphosphate (APP), a triazine macromolecular charring–foaming agent (CFA), and SiO$_2$ was applied to obtain an effective IFR–O-SEBS/PP system. The influences of a hot water treatment on the flame retardancy, water resistance, morphological structures, and mechanical properties were investigated through the limiting oxygen index (LOI), vertical burning test (UL-94), thermogravimetric analysis (TGA), cone calorimetry (CONE), scanning electron microscopy (SEM) and mechanical properties.

EXPERIMENTAL

Materials

SEBS (YH-503) was produced by Sinopec Baling Petrochemical Co., Ltd. (China). PP resin (homopolymer, melt flow rate = 3.5

Table II. LOI and UL-94 Data of the O-SEBS/PP/IFR Composites

Sample code	LOI (%)	UL-94 test	
		Dripping	UL-94 rating
A	17.2	Yes	Burning
B	30.8	No	V-0
C	31.2	No	V-0
D	32.4	No	V-0
E	29.5	Yes	Burning
F	27.6	Yes	Burning
G	28.0	Yes	Burning
H	29.6	Yes	Burning
I	35.6	No	V-0

g/10 min) was manufactured by Daqing Huake Co., Ltd. (China). APP (GD-101, crystalline form II, $n < 1500$, average particle size = 15 μm) was supplied by Zhejiang Longyou GD Chemical Industry Co., Ltd. (China). A triazine macromolecule,[29] used as a CFA, was produced by Heilongjiang Orient Science & Technology Co., Ltd.; it had an average particle size of 10 μm. Naphthenic oil (KN4010, flash point = 200°C) was purchased from Jinhua Kang Libo Lubricant Co., Ltd. (China). SiO$_2$ (50 nm) was obtained from Shanghai KaiYin Chemical Co., Ltd. (China), and an antidripping agent (SN3300) with an average particle size of 2 μm was offered by NanJing JiaYin Technology Co., Ltd. (China).

Preparation of the Samples

The IFR O-SEBS/PP composites were prepared by the blending of O-SEBS (SEBS containing 30 wt % naphthenic oil), PP, IFR, and the antidripping agent (SN3300). The weight ratio of O-SEBS to PP was 1:2. The IFRs for the composites consisted of APP, CFA, and SiO$_2$, in which the weight ratio of APP to CFA was from 2:1 to 5:1 and contained 5 wt % SiO$_2$ based IFR. All samples were mixed on a two-roll mill (Harbin Plastic Co., China) at 190–200°C for 10 min. After mixing, the samples
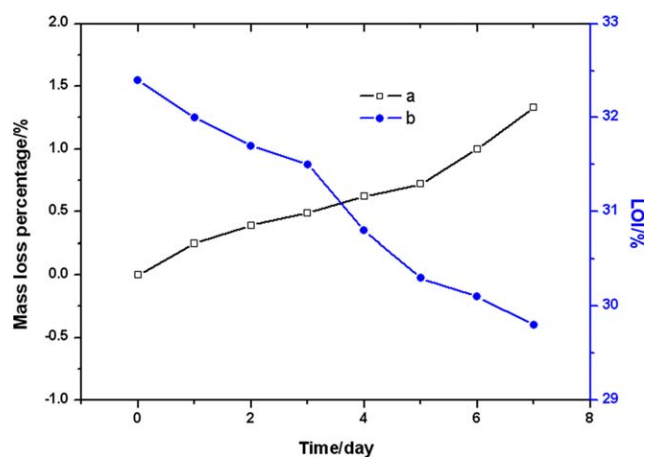

Figure 1. Burning testing and MLP of the water-treated IFR–O-SEBS/PP composites: (a) MLP (%) and (b) LOI (%). [Color figure can be viewed in the online issue, which is available at wileyonlinelibrary.com.]
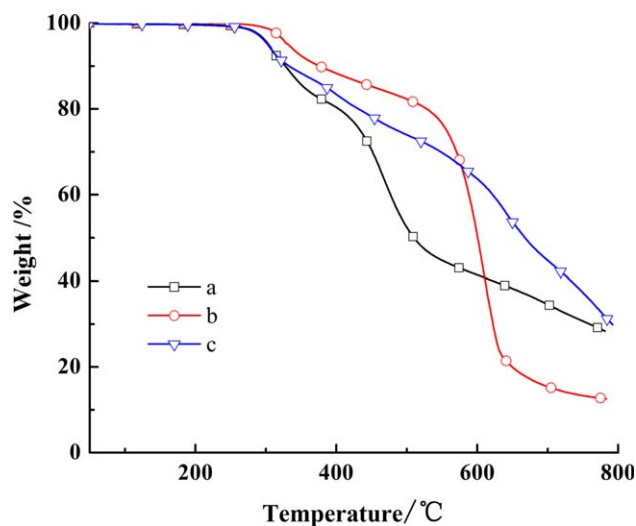
Figure 2. TGA curves of IFR and its components: (a) CFA, (b) APP, and (c) IFR. [Color figure can be viewed in the online issue, which is available at wileyonlinelibrary.com.]
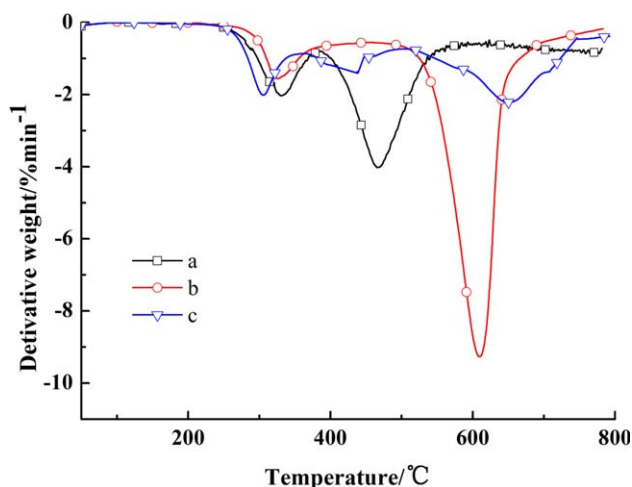

Figure 3. Differential thermogravimetry curves of IFR and its components: (a) CFA, (b) APP, and (c) IFR. [Color figure can be viewed in the online issue, which is available at wileyonlinelibrary.com.]

were hot-pressed under 10 MPa for 5 min at 190°C into sheets with suitable thicknesses by a hot-embossing machine (Harbin Plastic Co., China). The prepared sheets were cut into samples with a standard size and thickness for various analyses through

homemade molds with a cutting edge and a standard size. The size and thickness of the samples were dependent on the testing methods used in this study. The components of the IFR–O-SEBS/PP composites are listed in Table I.

Flame-Retardancy Tests

The LOI values of all of the samples were obtained at room temperature on a LOI instrument (JF-3) produced by JiangNing Analysis Instrument Factory (China) according to ISO4589-1984. The dimensions of the samples were $130 \times 6.5 \times 3$ mm^3.

The vertical burning tests were carried out on a CZF-2 instrument produced by JiangNing Analysis Instrument Factory. The dimensions of the samples were $125 \times 12.5 \times 1.6$ mm^3 according to the UL-94 standard. The UL-94 test results were classified by the burning ratings V-0, V-1, and V-2.

TGA

All TGA tests were carried out with a PerkinElmer Pyris 1 thermal analyzer at a linear heating rate of 10°C/min under pure nitrogen within the temperature range from 50 to 800°C. The weight of every sample was kept within 2–4 mg.

CONE Test

All CONE data were taken from a Fire Testing Technology cone calorimeter (West Sussex, United Kingdom) at an incident heat flux of 50 kW/m^2 according to ISO 5660-1. The samples ($100 \times 100 \times 3$ mm^3) were laid on a horizontal sample holder.

SEM

SEM was used to examine the morphology of the char residue obtained from CONE tests with a FEI QuanTa-200 SEM instrument (Eindhoven, The Netherlands). The accelerating voltage was set to 15 kV. The surface of the char residues was sputter-coated with a gold layer before examination.

Mechanical Properties Testing

Determinations of the tensile strength and elongation at break of all of the specimens were performed on Regeer computer-controlled mechanical instrument according to GB/T1040–1992. At least five specimens were tested for each sample, and the average values are reported.

Water Resistance Test

The IFR–O-SEBS/PP samples (1.6 mm thick) used for mass loss determination were weighed, and the weight was recorded as M_0. All of the samples were put into distilled water at 70°C, and the period lasted 1 to 7 days. The distilled water was

Table III. Thermal Degradation Data of IFR and Its Components

Samples	$T_{initial}$ (°C)	R_{1peak} (%/min min)/T_{1peak} (°C)	R_{2peak} (%/min)/T_{2peak} (°C)	R_{3peak} (%/min)/T_{3peak} (°C)	Char residue (%)	
					600°C	800°C
CFA	282	−2.0/331	−4.0/469	—	41	28
APP	297	−1.6/327	−9.3/610	—	50	13
IFR	263	−2.0/306	−1.4/438	−2.2/651	64	30

$T_{initial}$ = The initial thermal decomposition temperature when the mass loss is 1%. R_{1peak} = The mass loss rate of the first main thermal decomposition peak. T_{1peak} = The temperature of the first main thermal decomposition peak. R_{2peak} = The Mass loss rate of the second main thermal decomposition peak. R_{3peak} = The Mass loss rate of the third main thermal decomposition peak. T_{3peak} = The temperature of the third main thermal decomposition peak.
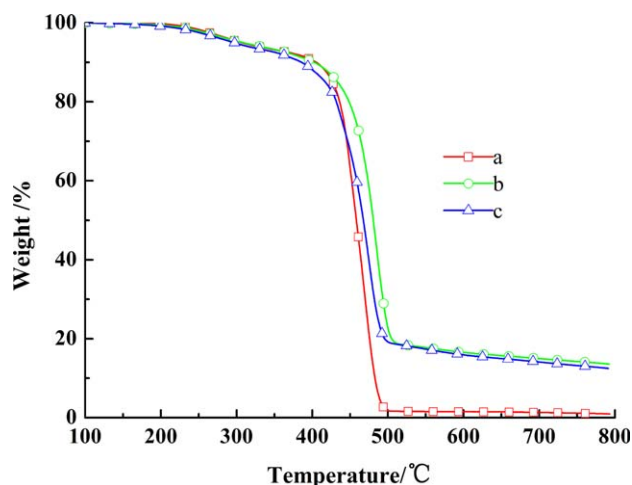
Figure 4. TGA curves of the blend and the IFR–O-SEBS/PP composites: (a) O-SEBS/PP composite (sample A), (b) IFR–O-SEBS/PP composites (sample D), and (c) water-treated IFR–O-SEBS/PP composites (sample T-D). [Color figure can be viewed in the online issue, which is available at wileyonlinelibrary.com.]
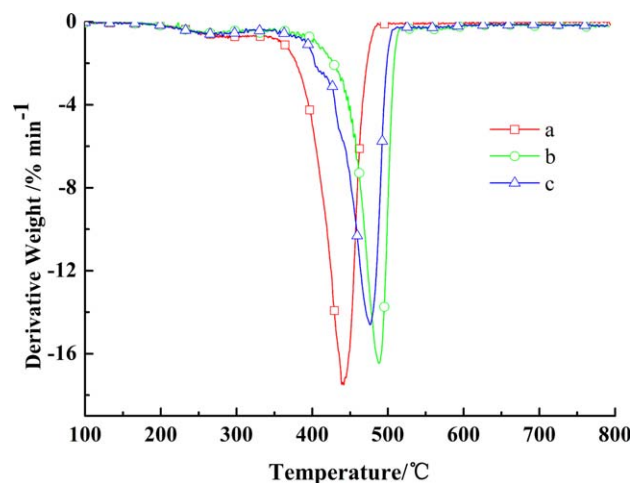

Figure 5. Differential thermogravimetry curves of the blend and the IFR–O-SEBS/PP composites: (a) O-SEBS/PP composite (sample A), (b) IFR–O-SEBS/PP composites (sample D), and (c) water-treated IFR–O-SEBS/PP composites (sample T-D). [Color figure can be viewed in the online issue, which is available at wileyonlinelibrary.com.]

replaced every 24 h, and then, the samples were dried at 80°C for 72 h and cooled to room temperature. The dried and treated samples were reweighed, and this weight was recorded

as M_1. The mass loss percentage (MLP) was calculated as follows:

$$MLP = [(M_0 - M_1)/M_0] \times 100\% \qquad (1)$$

The samples used for the LOI and UL-94 tests were also treated with the same method and are referred to as the water-treated IFR–O-SEBS/PP composite (sample T-D).

RESULTS AND DISCUSSION

Flame Retardancy

The effects of the triazine-macromolecule-containing IFR on the flame retardance of the O-SEBS/PP composites are shown in Table II. From the LOI values and UL-94 results of the O-SEBS/PP composite and the IFR–O-SEBS/PP composites, the O-SEBS/PP composite was very flammable, its LOI value was only 17.2%, and the UL-94 result was no rating. When the ratio of APP to CFA was kept at 4:1, with the increased IFR loading, the LOI values of the composites clearly increased. When the IFR loading reached 28 wt %, the LOI value increased to 32.4%, and the composite passed the UL-94 V-0 rating. This result indicates that the low IFR loading presented a high efficient flame retardancy in the O-SEBS/PP composites, despite the only 20–22 wt % IFR value for pure homopolypropylene.[29,30] Its flame-retardant efficiency was obviously higher than that of the metal hydroxides in the O-SEBS/PP composites reported in the literature.[13,15] At the same loading (28 wt %), with increasing APP/CFA ratio, the LOI values of the composites increased and then decreased. When the ratio of APP to CFA increased to 5:1, the composite failed to pass the UL-94 V-0 (1.6 mm) rating.

As potential applications in wire and cable materials, water-resistance abilities are an important property. Figure 1 gives the effects of the hot water treatment time on the MLP and flame retardancy of the IFR–O-SEBS/PP composite (sample D). With increasing water treatment time, MLP of the IFR–O-SEBS/PP composite increased slowly. When the water treatment time at 70°C reached 7 days and nights, MLP was only 1.33 wt % on the basis of the composite, the surface of the composite was smooth, and exudates did not appear. Because of the low MLP, the composite still passed UL-94 V-0 rating after water treatment, and its LOI value decreased to 29.8%. This result indicates the IFR exhibited excellent water resistance in the IFR–O-SEBS/PP composite. Compared with the water resistance of the IFR–PP composites reported in our previous work,[34] this

Table IV. Thermal Degradation Data of the O-SEBS/PP Composite and IFR–O-SEBS/PP Composites under Pure Nitrogen

Sample	$T_{initial}$ (°C)	R_{1peak} (%/min)/T_{1peak} (°C)	R_{2peak} (%/min)/T_{2peak} (°C)	Char residue (%) 600°C	800°C
A	234	0.8/289	18/441	2	1
D	208	0.6/264	16/488	17	14
T-D	208	0.7/276	15/476	16	13

$T_{initial}$ = The initial thermal decomposition temperature when the mass loss is 1%. R_{1peak} = The mass loss rate of the first main thermal decomposition peak. T_{1peak} = The temperature of the first main thermal decomposition peak. R_{2peak} = The Mass loss rate of the second main thermal decomposition peak.

Table V. CONE Data of the O-SEBS/PP and IFR–O-SEBS/PP Composites

	Sample		
Parameter	A	D	T-D
IT (s)	52	38	36
Peak HRR (kW/m^2)	916	266	255
THR (MJ m^{-2} kg^{-1})	103	91	96
Peak SPR (m^2/s)	0.11	0.05	0.05
TSP (m^2/kg)	16	16	17

IT = The ignition time of the samples during the CONE test.

IFR showed better water-resistance abilities in the IFR–O-SEBS/PP composite.

Thermal Degradation Behavior
The thermal degradation curves and data of the IFR and its components are given in Figures 2 and 3 and Table III. CFA, as a triazine macromolecular CFA, itself presented good thermal stability and charring ability. The char residue was 28 wt % at 800°C. APP, as a highly effective acid source, showed good thermal stability and a certain amount of P—O residue (13 wt %).[17] However, the thermal degradation behavior of the IFR was obviously different. First of all, the initial thermal decomposition temperature decreased to 263°C, and the char residue obviously increased. This result indicated that APP could catalyze CFA to form more char residue; in the IFR system consisting of CFA, APP, and SiO$_2$, SiO$_2$ was considered to stabilize the char layer, which was beneficial to the flame retardancy of the polymers.

Figures 4 and 5 and Table IV present the thermogravimetric analysis curves and data of the O-SEBS/PP blend, the IFR–O-SEBS/PP composite, and the water-treated IFR–O-SEBS/PP composite under pure nitrogen. All of the composites presented a little mass loss peak that took place between 260 and 290°C
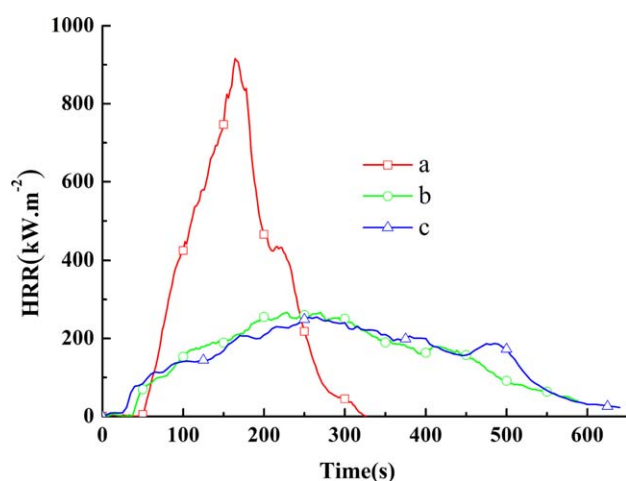

Figure 7. THR curves of the blend and the IFR–O-SEBS/PP composites: (a) O-SEBS/PP composite (sample A), (b) IFR–O-SEBS/PP composites (sample D), and (c) water-treated IFR–O-SEBS/PP composites (sample T-D). [Color figure can be viewed in the online issue, which is available at wileyonlinelibrary.com.]
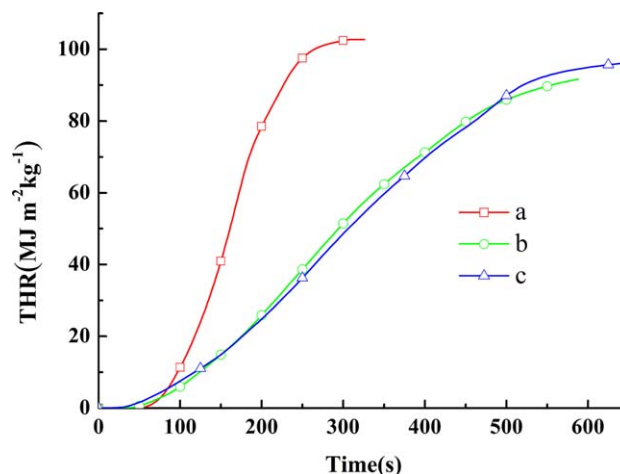
and a main thermal degradation temperature (T_{2peak}) occurring between 440 and 490°C. The initial thermal decomposition temperature of IFR was 263°C, as revealed in Figures 2 and 3 and Table III. The former was probably due to the decomposition of the IFR and the volatilization of naphthenic oil because of its flash point of 230°C. The latter was considered to be the thermal degradation of SEBS and the PP backbone and/or IFR. Compared with the O-SEBS/PP blend, the T_{2peak}'s of the IFR–O-SEBS/PP composite and the water-treated IFR–O-SEBS/PP composite clearly moved up. That is, T_{2peak} of the IFR–O-SEBS/PP composite reached 488°C, the amount of char residue was 14 wt % at 800°C, T_{2peak} of the water-treated O-SEBS/PP/IFR composite decreased to 476°C, and the char residue content was 13 wt %. These facts were understandable because the char layer
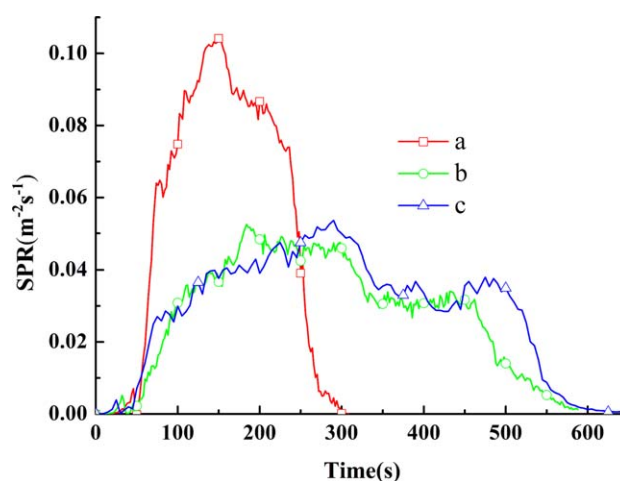

Figure 6. HRR curves of the blend and the IFR–O-SEBS/PP composites: (a) O-SEBS/PP composite (sample A), (b) IFR–O-SEBS/PP composites (sample D), and (c) water-treated IFR–O-SEBS/PP composites (sample T-D). [Color figure can be viewed in the online issue, which is available at wileyonlinelibrary.com.]

Figure 8. SPR curves of the blend and the IFR–O-SEBS/PP composites: (a) O-SEBS/PP composite (sample A), (b) IFR–O-SEBS/PP composites (sample D), and (c) water-treated IFR–O-SEBS/PP composites (sample T-D). [Color figure can be viewed in the online issue, which is available at wileyonlinelibrary.com.]
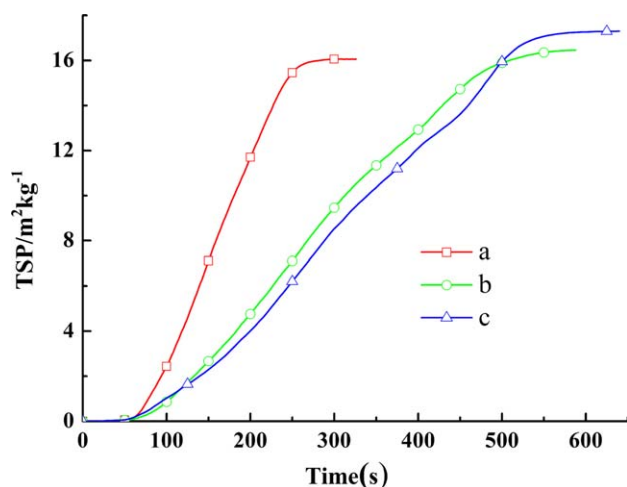
Figure 9. TSP curves of the blend and the IFR–O-SEBS/PP composites: (a) O-SEBS/PP composite (sample A), (b) IFR–O-SEBS/PP composites (sample D), and (c) water-treated IFR–O-SEBS/PP composites (sample T-D). [Color figure can be viewed in the online issue, which is available at wileyonlinelibrary.com.]

formed from the IFR decomposition could effectively protect the O-SEBS/PP composite from decomposing by the insulating heat effect of the char layer and prolong the time needed for the thermal degradation of the O-SEBS/PP composite. This result was similar to the thermal degradation behavior of the IFR–PP composite, which has been reported in the literature.[30] However, T_{2peak} of the water-treated IFR–O-SEBS/PP composite shifted to low temperature to a certain extent; this result was attributed to the fact that a small quantity of IFR was extracted from the IFR–O-SEBS/PP composite during the water-resistance test.

Flammability Behavior

Table V and Figures 6–10 present the data and curves of the various flammability parameters of the O-SEBS/PP blend, the
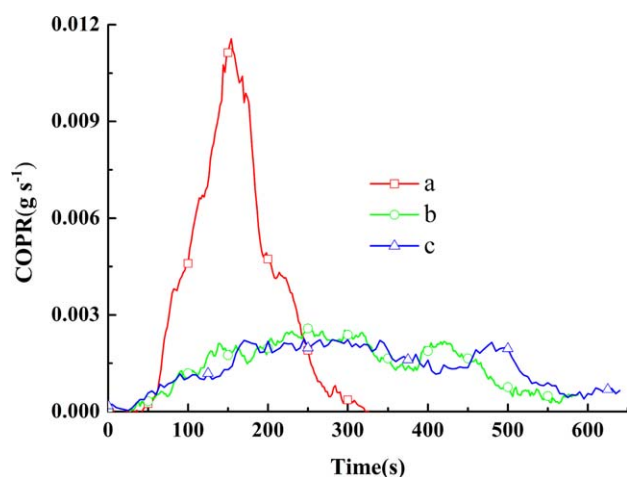

Figure 10. COPR curves of the blend and the IFR–O-SEBS/PP composites: (a) O-SEBS/PP composite (sample A), (b) IFR–O-SEBS/PP composites (sample D), and (c) water-treated IFR–O-SEBS/PP composites (sample T-D). [Color figure can be viewed in the online issue, which is available at wileyonlinelibrary.com.]
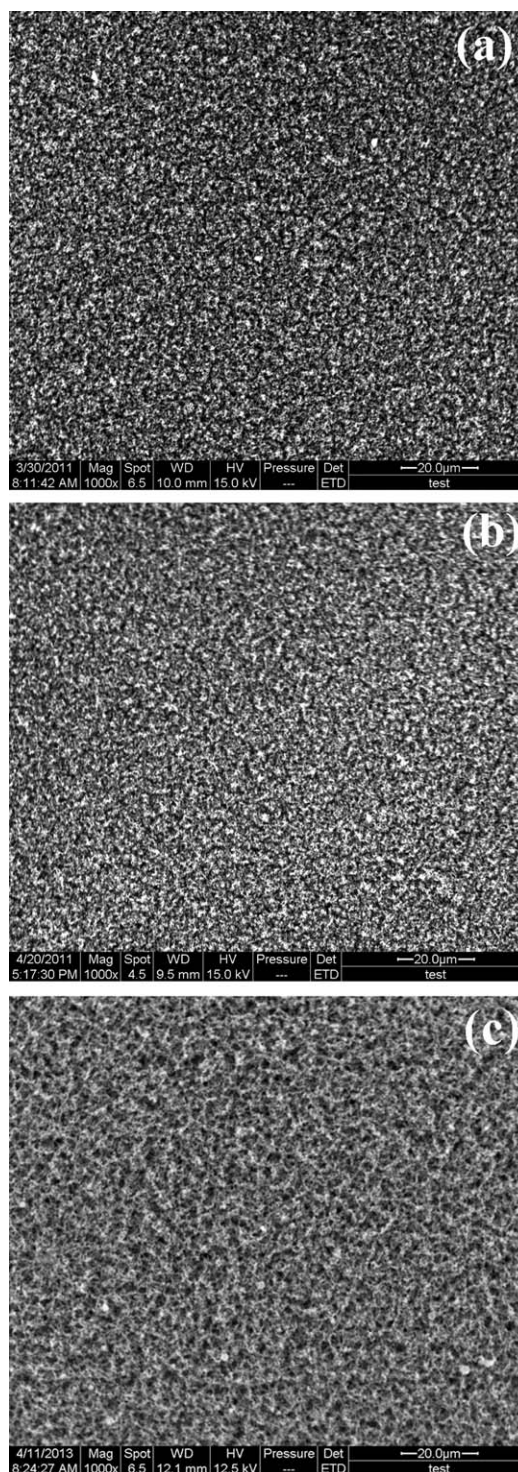

Figure 11. SEM photos of the char residues of the IFR–O-SEBS/PP composites: (a) IFR–O-SEBS/PP composites (sample D, 1000×), (b) water-treated IFR–O-SEBS/PP composites (sample T-D, 1000×), and (c) O-SEBS/PP composites (1000×).

IFR–O-SEBS/PP composite, and the water-treated IFR–O-SEBS/PP composite obtained from the CONE test at an incident heat flux of 50 kW/m². On the basis of the heat-release parameters [heat release rate (HRR) and total heat release (THR)], as revealed in Figures 6 and 7 and Table V, the blend burned very

Table VI. Mechanical Properties of the IFR–O-SEBS/PP Composites

Sample code	Tensile strength (MPa)	Elongation (%)
A	20.4	960
B	15.3	582
C	15.6	598
D	15.8	647
E	16.3	672
F	17.5	671
G	15.9	660
H	15.6	654
I	15.3	584
T-D	15.2	596

fast, its HRR peak value (peak HRR) was 916 kW/m^2, and its THR reached 103 MJ m^{-2} kg^{-1}. In contrast, the IFR–O-SEBS/PP composite and the water-treated IFR–O-SEBS/PP composite showed much lower HRR peak values. That is, the HRR peaks of IFR–O-SEBS/PP and the water-treated IFR–O-SEBS/PP composites decreased dramatically to 266 and 255 kW/m^2, respectively. This fact indicated that the water treatment rarely influenced the flammability behavior of the composite. This result was almost in agreement with the flame retardancy and TGA results discussed earlier. As shown in Table V, the IFR obviously shortened the ignition time; this was attributed to the char layer formation on the surface of the IFR–O-SEBS/PP composite. Because of the heat isolation of the char layer, which resulted in the blockage of heat transfer into the composite, and the quick increase in the temperature on the surface of the composite, the pyrolysis reactions took place quickly. This is a general characteristic of intumescent flame-retarded polymeric materials.[30,33,34]

The emissions of smoke and toxic gas (CO) are considered other important parameters for flame-retarded composites. The smoke production rate (SPR), total smoke production (TSP), and carbon monoxide production rate (COPR) of the O-SEBS/
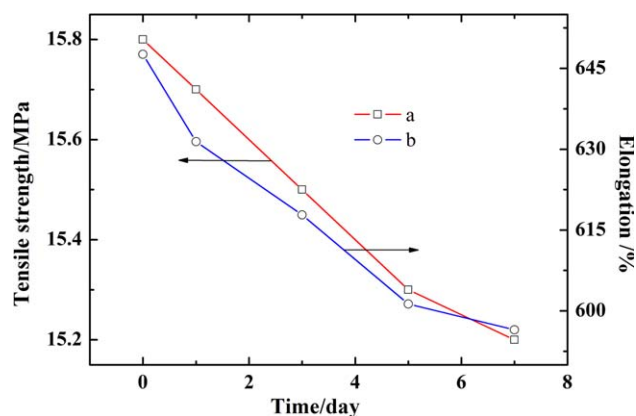

Figure 12. Mechanical properties of the IFR–O-SEBS/PP composites after water treatment: (a) tensile strength (MPa) and (b) elongation at break (%). [Color figure can be viewed in the online issue, which is available at wileyonlinelibrary.com.]
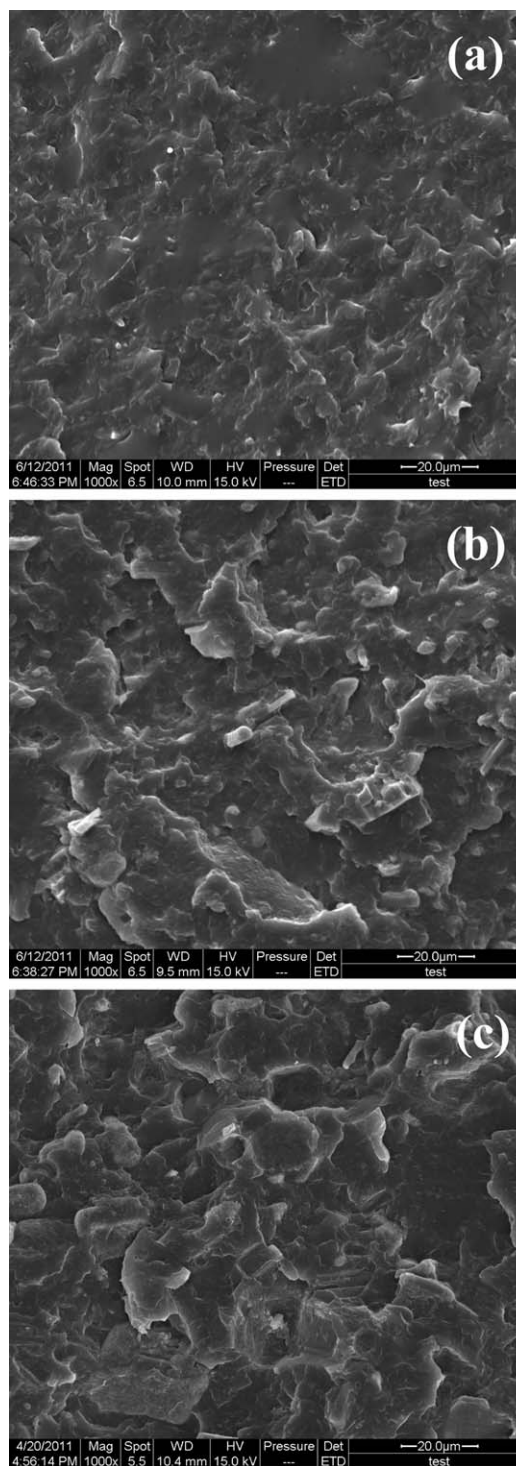

Figure 13. SEM of fracture of the IFR–O-SEBS/PP composites: (a) O-SEBS/PP composite (sample A, 1000×), (b) IFR–O-SEBS/PP composites (sample D, 1000×), and (c) water-treated IFR–O-SEBS/PP composites (sample T-D, 1000×).

PP blend, IFR–O-SEBS/PP composite, and water-treated IFR–O-SEBS/PP composite are shown in Table V and Figures 8–10. Similar to the HRR and THR curves, the SPR, TSP, and COPR values of the IFR–O-SEBS/PP composite and water-treated

IFR–O-SEBS/PP composite were significantly reduced compared with those of the O-SEBS/PP blend. The smoke emission process obviously slowed compared with that of the blend.

Figure 11 shows the morphological structures of the char residues of the IFR–O-SEBS/PP composite, the water-treated IFR–O-SEBS/PP composite (samples D and T-D), and the O-SEBS/PP composite obtained from the CONE test. As revealed in Figure 11(c), the surface morphological structure of the char residues of the O-SEBS/PP composite was not compact and homogeneous, and there were many holes and cavities. The morphological structure of the char residues of the IFR–O-SEBS/PP composite [Figure 11(a)] was homogeneous and compact. The char residue was likely formed by a series of reactions of dehydration and crosslinking of the CFA particles catalyzed by APP, like a system of pentaerythritol charring catalyzed by APP.[17,18,34] Compared with the IFR–O-SEBS/PP composite, we also observed that the morphological structure of the char residues of the water-treated IFR–O-SEBS/PP composite [Figure 11(b)] was the same as that of the IFR–O-SEBS/PP composite. This indicated that water treatment almost did not influence the morphological structures of the char residues of the composites. This result also nearly further explained the same flame retardancy and flammability behavior of the IFR–O-SEBS/PP composite and the water-treated IFR–O-SEBS/PP composite.

Mechanical Properties and Interface Morphology

The tensile strength and elongation at break of the blend, IFR–O-SEBS/PP composite, and water-treated IFR–O-SEBS/PP composite are given in Table VI and Figure 12. We observed that at the same loading of the IFR, with increasing mass ratio of APP to CFA, the tensile strength and elongation at break of the composites showed little change. In addition, with increasing IFR loading, the tensile strength and elongation at break of the composites decreased gradually. When the addition of the IFR was 28 wt % in the O-SEBS/PP composite, the tensile strength and elongation decreased to 15.8 MPa and 647%, respectively. According to Figure 12, with increasing hot water treatment time, the tensile strength only decreased from 15.8 to15.2 MPa, and the elongation at break decreased from 647 to 596%, respectively. This result indicated that the water-treated IFR–O-SEBS/PP composite still retained good mechanical properties.

Figure 13 shows the SEM micrographs of the fractured surfaces of the O-SEBS/PP composite, the IFR–O-SEBS/PP composite, and the water-treated O-SEBS/PP/IFR composite. O-SEBS and PP presented good interfacial compatibility, as revealed in Figure 13(a). The IFR could uniformly distribute in the O-SEBS/PP composite, as shown in Figure 13(b,c). As shown in Figure 13(c), holes produced for the extract of the IFR did not appear, but the IFR still could uniformly distribute in the IFR–O-SEBS/PP composite. This fact further proved that the water-treated IFR–O-SEBS/PP composite still retained good mechanical properties.

CONCLUSIONS

A flame-retardant and water-resistant O-SEBS/PP composite was developed in this study. The results indicate that the optimal flame-retardant formulation was APP/CFA = 4:1, which sat-isfied a UL-94 V–0 rating (1.6 mm) and a high LOI value (32.4%) when the loading of IFR was 28 wt %. The IFR–O–SEBS/PP composite presented excellent water resistance, and the water-treated IFR–O–SEBS/PP composite could still pass a UL–94 V–0 (1.6 mm) rating. On the basis of the HRR and SPR of all of the IFR composites from CONE, we also demonstrated that the IFR presented effective flame retardancy and excellent water resistance in the IFR–O–SEBS/PP composite. The water treatment almost did not affect the morphological structures of the char residue and fractured surfaces of the composites and the mechanical properties of the composite. This novel IFR–O-SEBS/PP composite should present potential applications in wires and cables.

REFERENCES

1. Liao, C. Z.; Tjong, S. C. *Polym. Eng. Sci.* **2011**, *51*, 948.

2. Wonchalerm, R.; Masaya, K.; Takuma, S.; Go, K.; Shinichi, S.; Suwabun, C. *Polymer* **2011**, *52*, 844.

3. White, C. C.; Tan, K. T.; Hunston, D. L.; Nguyen, T.; Benatti, D.; Stanley, J. D.; Chin, J. W. *Polym. Degrad. Stab.* **2011**, *96*, 1104.

4. Juárez, D.; Ferrand, S.; Fenollar, O.; Fombuena, V.; Balart, R. *Eur. Polym. J.* **2011**, *47*, 153.

5. Radhakrishnan, C. K.; Sujith, G.; Unnkrishnan, G. *J. Polym. Res.* **2008**, *15*, 161.

6. Anirban, G.; Mousumi, D. S. *J. Appl. Polym. Sci.* **2006**, *100*, 2040.

7. Anirban, G.; Bhowmick, A. K. *J. Mater. Sci.* **2009**, *44*, 903.

8. Xu, W.; Cheng, Z. P.; Zhang, Z. B.; Zhang, L. F.; Zhu, X. L. *React. Funct. Polym.* **2011**, *71*, 634.

9. Ma, Z, S.; Jiang, P, K.; Wang, L. C. *J. Appl. Polym. Sci.* **2010**, *118*, 2350.

10. Abreu, F.; Liberman, S. A. *J. Appl. Polym. Sci.* **2005**, *95*, 254.

11. Onur, B.; Ayhan, E.; Halil, D. *Polym. Compos.* **2010**, *31*, 1265.

12. Shigeki, H.; Kazuya, N.; Kenji, M. *J. Appl. Polym. Sci.* **2009**, *114*, 919.

13. Xiao, W. D.; Kibble, K. A. *Polym. Polym. Compos.* **2008**, *16*, 415.

14. Zhao, J. Q.; Ge, J. J.; Liu, S. M.; Wu, S. Z. Chin. Pat. CN 101629007A (**2009**).

15. Wang, Z.; Li, H, C.; Wang, T. Chin. Pat. CN 1970610A (**2007**).

16. Hao, D. M.; Liu, Y. M.; Chen, C. W. Chin. Pat. CN 101469100A (**2009**).

17. Camino, G.; Costa, L.; Trossarelli, L. *Polym. Degrad. Stab.* **1984**, *6*, 243.

18. Camino, G.; Costa, L.; Trossarelli, L. *Polym. Degrad. Stab.* **1985**, *12*, 203.

19. Bras, M. L.; Bourbigot, S.; Félix, E.; Pouille, F.; Siat, C.; Traisnel, M. *Polymer* **2000**, *41*, 5283.

20. Li, L. Y.; Chen, G. H.; Liu, W.; Li, J. F.; Zhang, S. *Polym. Degrad. Stab.* **2009**, *94*, 996.

21. Huang, G. B.; Gao, J. R.; Li, Y. J.; Han, L.; Wang, X. *Polym. Degrad. Stab.* **2010**, *95*, 245.

22. Ribeiro Simone, P. S.; Estevao Luciana, R. M.; Pereira, C.; Rodrigues, J.; Nascimento Regina, S. V. *Polym. Degrad. Stab.* **2009**, *94*, 421.

23. Lin, M.; Li, B.; Li, Q. F.; Li, S.; Zhang, S. Q. *J. Appl. Polym. Sci.* **2011**, *121*, 1951.

24. Li, B.; Jia, H.; Guan, L. M.; Bing, B. C.; Dai, J. F. *J. Appl. Polym. Sci.* **2009**, *114*, 3626.

25. Wang, K.; Wang, Z. Z.; Liu, H. *J. Polym. Compos.* **2008**, *29*, 844.

26. Liu, Y.; Feng, Z. Q.; Wang, Q. *Polym. Compos.* **2009**, *30*, 221.

27. Liu, Y.; Wang, Q. *Polym. Compos.* **2007**, *28*,163.

28. Wang, J. C.; Chen, Y. H. *Elastomers Plast.* **2007**, *39*, 33.

29. Li, B.; Xu, M. *J. Polym. Degrad. Stab.* **2006**, *91*, 1380.

30. Dai, J. F.; Li, B. *J. Appl. Polym. Sci.* **2010**, *116*, 2157.

31. Wang, Z. Z.; Lv, P.; Hu, Y.; Hu, K. L. *J. Anal. Appl. Pyrol.* **2009**, *86*, 207.

32. Zhang, S. Q.; Li, B.; Li, M.; Li, Q. F.; Gao, S. L.; Yi, W. *J. App. Polym. Sci.* **2011**, *122*, 3430.

33. Li, Y. T.; Li, B.; Dai, J. F. *Polym. Degrad. Stab.* **2008**, *93*, 9.

34. Gao, S. L.; Li, B.; Bai, P.; Zhang, S. Q. *Polym. Adv. Technol.* **2011**, *22*, 2609.